ADVANCED MATERIALS
www.advmat.de

# Natural Hydrogels Support Kidney Organoid Generation and Promote In Vitro Angiogenesis

*Elena Garreta,* Daniel Moya-Rull, Andrés Marco, Gaia Amato, Asier Ullate-Agote, Carolina Tarantino, Maria Gallo, David Esporrín-Ubieto, Alberto Centeno, Amaia Vilas-Zornoza, Rafael Mestre, María Kalil, Izar Gorroñogoitia, Ane Miren Zaldua, Samuel Sanchez, Laura Izquierdo Reyes, María Eugenia Fernández-Santos, Felipe Prosper, and Nuria Montserrat**

**To date, strategies aiming to modulate cell to extracellular matrix (ECM) interactions during organoid derivation remain largely unexplored. Here renal decellularized ECM (dECM) hydrogels are fabricated from porcine and human renal cortex as biomaterials to enrich cell-to-ECM crosstalk during the onset of kidney organoid differentiation from human pluripotent stem cells (hPSCs). Renal dECM-derived hydrogels are used in combination with hPSC-derived renal progenitor cells to define new approaches for 2D and 3D kidney organoid differentiation, demonstrating that in the presence of these biomaterials the resulting kidney organoids exhibit renal differentiation features and the formation of an endogenous vascular component. Based on these observations, a new method to produce kidney organoids with vascular-like structures is achieved through the assembly of hPSC-derived endothelial-like organoids with kidney organoids in 3D. Major readouts of kidney differentiation and renal cell morphology are assessed exploiting these culture platforms as new models of nephrogenesis. Overall, this work shows that exploiting cell-to-ECM interactions during the onset of kidney differentiation from hPSCs facilitates and optimizes current approaches for kidney organoid derivation thereby increasing the utility of these unique cell culture platforms for personalized medicine.**

## 1. Introduction

The human kidney is one of the most complex organs with an elaborate and arborized architecture containing more than 23 differentiated cell types anatomically organized in distinct segments, including vascular, interstitial, collecting duct, and nephron compartments.[1–3] It performs central physiological functions including the removal of the metabolic waste products of our body and the maintenance of the extracellular homeostatic balance of tissue fluids.[4] In this regard, chronic kidney disease (CKD)-related diseases remain one of the major global health issues affecting around 10% of the world population.[5,6] One of the major roadblocks in developing therapies for CKD has been the lack of reliable preclinical models. The use of animal models has limited utility to study CKD because they fail to recapitulate important functional, structural, and molecular

E. Garreta, D. Moya-Rull, A. Marco, G. Amato, C. Tarantino, M. Gallo, M. Kalil, N. Montserrat
Pluripotency for Organ Regeneration
Institute for Bioengineering of Catalonia (IBEC)
Barcelona Institute of Science and Technology (BIST)
Carrer de Baldiri i Reixac, 15–21, Barcelona 08028, Spain
E-mail: egarreta@ibecbarcelona.eu; nmontserrat@ibecbarcelona.eu
E. Garreta
University of Barcelona
Barcelona 08028, Spain

The ORCID identification number(s) for the author(s) of this article can be found under https://doi.org/10.1002/adma.202400306



**DOI: 10.1002/adma.202400306**

A. Ullate-Agote, A. Vilas-Zornoza
Regenerative Medicine Program, Centre for Applied Medical Research (CIMA)
Universidad de Navarra, Instituto de Investigación Sanitaria de Navarra (IdiSNA)
Pamplona 31008, Spain
D. Esporrín-Ubieto, R. Mestre, S. Sanchez
Institute for Bioengineering of Catalonia (IBEC)
Barcelona Institute of Science and Technology (BIST)
Carrer de Baldiri i Reixac, 10–12, Barcelona 08028, Spain
A. Centeno
Instituto de Investigación Biomédica de A Coruña (INIBIC)
Complexo Hospitalario Universitario A Coruña (CHUAC), Sergas
Universidade da Coruña (UDC)
As Xubias, A Coruña 15006, Spain
I. Gorroñogoitia, A. M. Zaldua
Leartiker S. Coop
Xemein Etorbidea 12A, Markina-Xemein 48270, Spain
S. Sanchez
Catalan Institute for Research and Advanced Studies (ICREA)
Passeig de Lluís Companys 23, Barcelona 08010, Spain

features of advanced human kidney disease. In this context, in vitro 3D cultures of kidney organ-like structures, so-called kidney organoids, represent an attractive alternative for kidney disease modeling and have the advantage of being scalable for drug or genetic screens.[7,8]

In recent years, most of the initial organoid procedures transformed aggregates of progenitor cells [either of human pluripotent stem cells (hPSCs)- or adult stem cells- origin] into versions of multiple simple to complex organs using extracellular matrix (ECM)-derived hydrogels. To date, Matrigel has been the most widely used matrix for these purposes with only a few studies exploring other solid ECMs, as collagen type I for organoid derivation.[9] On the other hand, in current hPSC-derived organoid systems (including brain, gut, blood vessels, inner cell ear, among others), the niche components are reproduced because of intrinsic cell-cell and cell-ECM interactions together with the addition of external components including growth factors, small molecules, and ECM matrices.[10] A different strategy has been adopted for the derivation of kidney organoids in where the most common culture procedures for organoid assembly and culture largely exploit the transwell cell culture system to support organoid differentiation in the absence of external ECM components.[11–13]

During organ development, the ECM behaves as a natural scaffolding that tightens the integrating vasculature.[14] Indeed, compelling work has demonstrated the impact of mutations in several ECM components in vasculogenesis (reviewed in ref. [14]), thus proving the role of organ ECM in this process. Furthermore, the vascular function becomes increasingly specialized in the time course of organ development.[15] In this regard, organ-derived decellularized ECM (dECM) are envisioned as unique biomaterials to recreate stem-cell-like niches providing key elements to control the regulation of stem cell fate and function.[16] We and others have recently exploited these properties combined with hPSCs to re-construct hPSC-derived tissue-like analogs using human organ derived dECMs.[17] Other works have partially or totally reconstructed human organs through the combination of organ derived dECMs and hPSC-differentiated cells.[18–20] With regard to kidney differentiation, previous works have investigated the potential role of rhesus monkey kidney-derived dECMs as external inducers of renal commitment from human embryonic stem cells (hESCs).[21,22] Other studies showed that acellular mouse kidney ECMs sustained differentiation of mouse embryonic stem cell (mESC)-derived renal progenitors[23] and hPSC-derived renal progenitor cells and endothelial cells.[24] Accumulative research has shown the unique role of dECM to act as a bioactive reservoir of growth factors such as EGF, FGF, and VEGF (reviewed in ref. [25]). In this regard, kidney-derived hydrogels together with the use of soluble VEGF have been recently shown to act as a primary source of vascularization during hPSC-kidney organoid derivation. However, the potential benefit of the sole use of kidney-specific ECM proteins to favor hPSC-kidney organoid derivation and vascularization remains to be revealed. Here, we define the development and characterization kidney dECM-derived hydrogels. We next explore the application of these biomaterials to qualitatively and quantitively promote kidney organoid differentiation and vascularization. Furthermore, we demonstrate the angiogenic potential of these biomaterials by their transplantation in the chick chorioallantoic membrane (CAM). These results prove the amenability of kidney dECM-derived hydrogels to leverage the ability of hPSC-derived renal progenitor cells to robustly self-organize and give rise to complex multicellular structures, including a vascular component. Based on these observations we have defined a straightforward approach for the generation of kidney-endothelial assembloids including a vascular component. Our findings provide insights into kidney organoid morphogenesis and ECM interactions, and a basis for the development of novel procedures for kidney organoid vascularization for immediate applications for organoid transplantation in clinically relevant environments as well as for investigations on vascular dysfunction during human disease.

## 2. Results and Discussion

### 2.1. Generation and Characterization of Porcine Kidney Extracellular Matrix-Derived Hydrogels

We first established the optimal conditions to efficiently decellularize kidney cortical tissue from pigs, a protocol that lasted 14 days (**Figure 1**A–E and Figure S1A–E, Supporting Information). To that we designed a 5-step protocol which includes i) tissue harvesting; ii) decellularization; iii) freeze dry and milling; iv) enzymatic digestion; and v) neutralization based on modification of previously reported protocols[26–29] (Figure 1A–D). Original tissue (native sample) was also used for further histological characterization (Figure S1A, Supporting Information), and the assessment of ECM and renal markers expression (Figure 1E and Figure S1B, Supporting Information). This short protocol minimized morphological tissue alteration compared to other decellularization protocols. This was confirmed by the preservation of renal morphology and major ECM components after decellularization such as collagen, basement membrane proteins, and elastin using different histological stainings (Figure S1A,

L. Izquierdo Reyes
Urology Department
Hospital Clinic of Barcelona
Barcelona 08036, Spain

M. E. Fernández-Santos
Department of Cardiology
Hospital General Universitario Gregorio Marañón
Madrid 28009, Spain

M. E. Fernández-Santos
ATMPs Production Unit
Instituto de Investigación Sanitaria Gregorio Marañón (IiSGM)
Madrid 28009, Spain

F. Prosper
Hematology Service and Cell Therapy Unit and Program of Hematology-Oncology CIMA-Universidad de Navarra
Cancer Center Clínica Universidad de Navarra (CCUN) and Instituto de Investigación Sanitaria de Navarra (IdISNA)
Pamplona 31008, Spain

F. Prosper
Centro de Investigación Biomedica en Red de Oncología (CIBERONC) and RICORS TERAV
Madrid 28029, Spain

N. Montserrat
Catalan Institute for Research and Advanced Studies (ICREA)
Passeig de Lluís Companys 23, Barcelona 08010, Spain

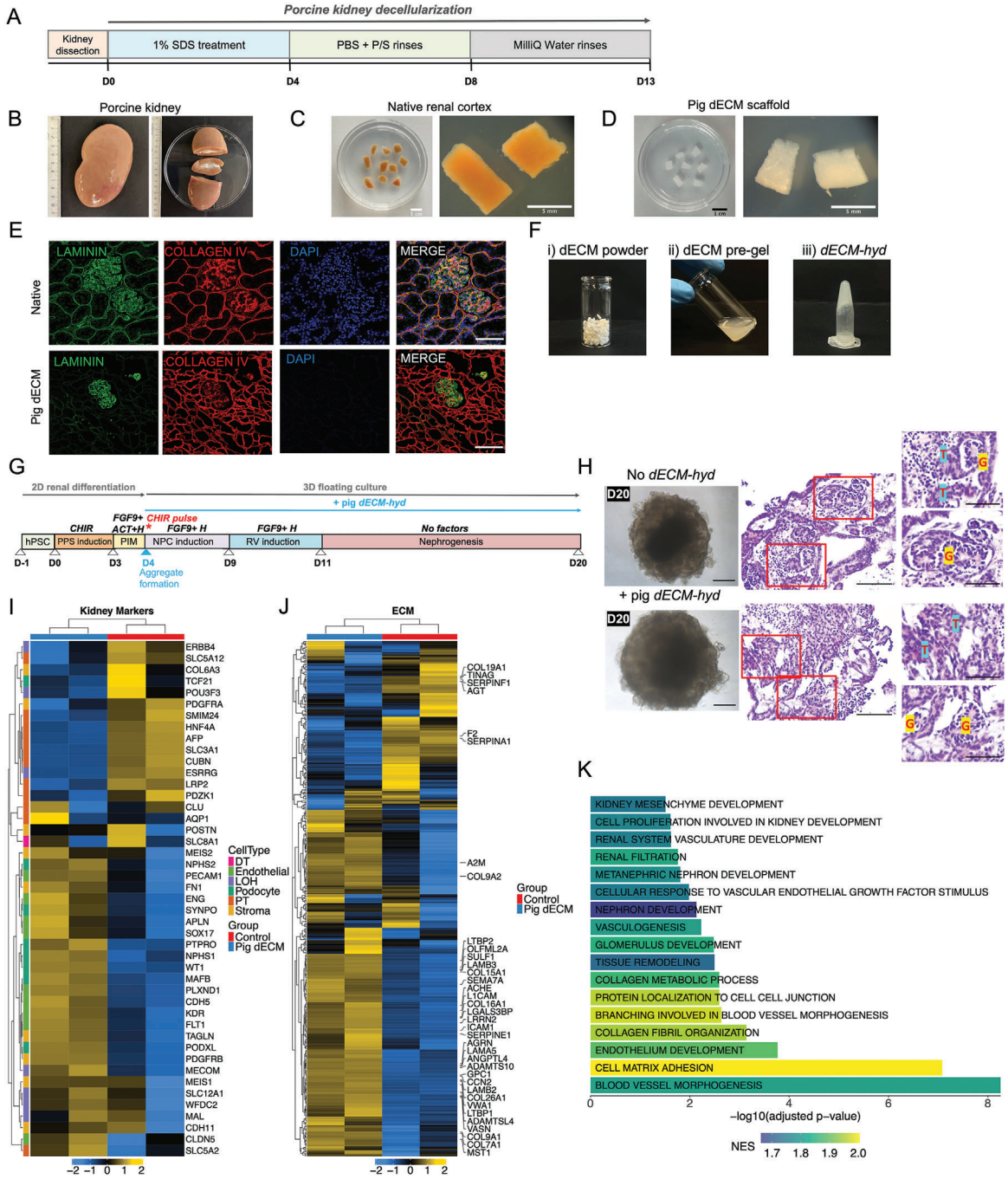


**Figure 1.** Generation of porcine kidney dECM hydrogel for kidney organoid differentiation. A) Schematic of the protocol for porcine kidney decellularization. B) Representative photograph of a pig kidney before decellularization. C) Pig renal cortical tissue pieces before decellularization. D) Pig renal cortical tissue pieces after decellularization. Scale bars, 1 cm, 5 mm (magnified views). E) Immunohistochemical analysis of native and decellularized renal tissue for the detection of LAMININ (green), COLLAGEN IV (red), and the nuclei staining DAPI (blue). Scale bars, 100 µm. F) Representative images of i) the dECM powder, ii) the pre-gel solution obtained after the enzymatic digestion of the dECM powder, and iii) the *dECM-hyd* resulting from gelation of the pre-gel at 37 °C. G) Experimental scheme for the generation of kidney organoids from hPSCs in the presence of porcine kidney *dECM-hyd* diluted in the medium. H) Representative bright field images, and hematoxylin and eosin staining of kidney organoids generated in the presence (+pig *dECM-hyd*) or absence (No *dECM-hyd*) of porcine *dECM-hyd*. Glomeruli-like structures are indicated with "G." Tubule-like structures are indicated with "T." Scale bars, 100, 50 µm (magnified views). I) Heatmap representing scaled values for normalized bulk RNA-seq gene expression of markers from different kidney cell-types in +pig *dECM-hyd* cultured organoids compared to No *dECM-hyd* cultured counterparts (control). J) Heatmap representing scaled values for normalized bulk RNA-seq gene expression of extracellular matrix genes in +pig *dECM-hyd* cultured organoids compared to No *dECM-hyd* cultured counterparts (control). Differentially expressed genes are labeled. K) Bar plot representing a selection of significant GO Biological processes upregulated in a gene set enrichment analysis in +pig *dECM-hyd* cultured organoids compared to No *dECM-hyd* cultured counterparts (control). Bars are colored by normalized enrichment score (NES) value. See also Figure S1, S2 and S3, Supporting Information.

Supporting Information), as reported in previous studies.[26–29] Consecutive paraffin sections were next assayed using immunohistochemistry against basement membrane proteins, such as LAMININ and COLLAGEN IV, and the nuclei stain DAPI further revealing the retention of basement membrane proteins in decellularized renal tissue scaffolds similarly to those in the native pig kidney (Figure 1E and Figure S1B, Supporting Information). DAPI staining was not visible in dECMs, indicating the loss of cellular material (Figure 1E and Figure S1B, Supporting Information) and further demonstrating that successive cycles of the 1% SDS detergent treatment for 4 days facilitated nuclei removal and significant DNA decrease as residual DNA content in dECMs were below 3% (Figure S1C, Supporting Information). Moreover, quantification of collagen and elastin content resulted in the presence of these components after tissue decellularization (Figure S1D,E, Supporting Information). Soluble collagen and elastin content measured in dECMs were comparable to the values found in the native tissue (Figure S1D,E, Supporting Information) in accordance with previous studies using SDS for decellularization.[30] The detection of the alpha-galactosidase (alpha-GAL) antigen was also evaluated in pig dECMs demonstrating its absence compared to the native tissue (Figure S1B, Supporting Information). Overall, our results suggested that the decellularization procedure developed here supports the derivation of porcine renal dECM scaffolds that fulfill the established criteria of decellularization.[16]

Next pig renal dECMs were enzymatically digested with pepsin in acidic conditions for 72 h at room temperature (RT) to produce a 3% (w/v) dECM pre-gel solution (Figure 1F). The thermoresponsive behavior of dECM hydrogels (*dECM-hyd*) was studied by the inverted tube method (Figure 1F; see Experimental Section), indicating that *dECM-hyd* behaved as a weak gel upon heating to 37 °C. We next confirmed the presence of collagens in *dECM-hyd* by second harmonic generation (SHG) two-photon microscopy, showing the detection of a dense fibrillary collagen component (Figure S1F, Supporting Information). Subcellular physical features of a scaffold determine a range of cell behaviors including morphology, cytoskeletal organization, migration, matrix remodeling, and long-range force transmission, among others.[31] For this reason, we also analyzed *dECM-hyd* microstructure by scanning electron microscopy (SEM) revealing that *dECM-hyd* was composed of a densely packed interconnected fibrous network (Figure S1G, Supporting Information).

Collagen and fibrin are essential components of the ECM and play a central role during in vivo angiogenic processes. Such properties have started to be investigated for the definition of new vascularization strategies and to develop in vitro microenvironments for tissue engineering and disease modeling.[31] In this regard, accumulative efforts have been directed toward the development of angiogenic biomaterial platforms incorporating elements of the vascular niche or facilitating its development for applications in mechanistic studies defining how vasculature influences cancer progression and therapy. Here we investigated the angiogenic capacity of the generated dECM biomaterials for further applications on hPSC-kidney organoid generation and vascularization. In recent years, the chick CAM has emerged as a naturally in vivo microenvironment to study angiogenesis (or its inhibition) in response to tissues, cells, or soluble factors. Other studies have collectively shown that the CAM represents a minimally invasive assay to assess the biocompatibility of materials for tissue engineering or regenerative medicine. In light of all these findings, we modified our recently developed procedure to assess hPSC-kidney organoid vascularization by exploiting the CAM assay[13] to detect the endogenous angiogenic potential of our dECM biomaterials (Figure S1H, Supporting Information). To that, biomaterials composed of 3% (w/v) *dECM-hyd* and 2 mg $mL^{-1}$ collagen I (1:3) were implanted into the CAM of 7-day-old chick embryos for 4 days. Collagen I hydrogels (without *dECM-hyd* supplementation) were used as control counterparts. Our results showed that on day 4 of implantation, multiple blood vessels from the CAM were macroscopically distinguished throughout the hydrogel supplemented with *dECM-hyd* in comparison with the collagen I hydrogel alone (Figure S1I, Supporting Information). At this stage, *in ovo* intravital injection of dextran-FITC (fluorescein isothiocyanate) into the CAM vasculature allowed for live imaging and quantitative analysis of the blood vessels surrounding the engrafted materials (Figure S1I,J, Videos S1 and S2, Supporting Information), which showed biocompatibility and angiogenic capacity (Figure S1J, Supporting Information).

### 2.2. Porcine Kidney Extracellular Matrix-Derived Hydrogels Sustain Kidney Organoid Differentiation from hPSCs

ECM scaffolds provide a cell-instructive structural framework(s) that induce the differentiation cells of different origins. Supporting this hypothesis, early works already showed that the coculture of hPSCs with renal ECM scaffolds can promote the expression of early renal markers.[21,22,24] In the light of these previous findings, we further explored the potential use of *dECM-hyd* as biological matrices supporting hPSC commitment and differentiation to renal progenitor cells and nephron-like complex structures. Toward this aim, we first defined a directed differentiation protocol for the derivation of renal progenitor cells (Figure 1G; see Experimental Section). Briefly, hPSCs cultured in a monolayer format were initially exposed to inductive signals promoting the generation of posterior primitive streak (PPS) using a high dose of the GSK3$\beta$ inhibitor, CHIR99021 (CHIR; 8 μM), to activate canonical Wnt signaling, for 3 consecutive days. To further promote the generation of posterior intermediate mesoderm (PIM), on day 3 cultures were subsequently supplemented with FGF9 and Activin A (20:1) for 1 additional day. On day 4, cell culture monolayers were exposed to a single dose of CHIR (5 μM) for 1 h to further activate Wnt signaling to promote the epithelialization of renal mesodermal progenitors. qPCR analysis during the time course of PIM induction showed the upregulation of the intermediate mesoderm (IM) markers including OSR1, PAX2, and LHX1, the PIM marker HOXD11, and the anterior IM marker GATA3 (Figure S1K, Supporting Information). Moreover, immunofluorescence and confocal analysis on day 4 showed the efficient generation of densely packed cell monolayers expressing the IM marker PAX2 (Figure S1L, Supporting Information) that further differentiated in the presence of FGF9 into nephron progenitor cells (NPCs) expressing PAX2 and WT1 on day 9 (Figure S1M, Supporting Information).

To test the potential of pig kidney *dECM-hyd* to support kidney organoid generation, PIM-committed cell monolayers were

further differentiated in combination with pig *dECM-hyd* in free-floating 3D culture conditions (Figure 1G; see Experimental Section). For this aim day 4 PIM cells were dissociated and spun centrifugated to force the generation of spheroids using V-bottom 96 multi-well plates. At this point of the protocol, pig *dECM-hyd* was supplemented in the medium at 1:40 dilution (0.075% w/v of *dECM-hyd*) until day 20 of differentiation with medium changes every other day. PIM-derived spheroids in the absence of *dECM-hyd* supplementation were used as control counterparts. From days 4 to 11 PIM-derived spheroids were cultured in the presence of FGF9 after which FGF9 was removed, and organoids were allowed to differentiate without the addition of any growth factors until day 20. This methodology efficiently resulted in the generation of hPSC-kidney organoids with segmented nephron-like structures containing podocyte-like and tubular-like cells in both experimental conditions as shown by hematoxilin and eosin staining in organoid paraffin sections (Figure 1H), and immunofluorescence analysis for well-known kidney markers for podocyte (NEPHRIN, WT1, PODXL), proximal tubule (*Lotus Tetraglobus lectin* [LTL]) and distal tubule [E-CADHERIN (ECAD)] differentiation (Figure S2, Supporting Information). To understand the impact of pig *dECM-hyd* in kidney organoid differentiation, we performed bulk RNA sequencing (RNA-seq) in day-20 kidney organoids generated in the presence of pig *dECM-hyd* compared to control conditions. Differential gene expression analysis showed increased expression of podocyte-related (e.g., NPHS2, SYNPO, PODXL, MAFB) and endothelial differentiation (PECAM1, KDR, ENG) markers in pig *dECM-hyd*-cultured organoids compared to control conditions (Figure 1I and Table S1, Supporting Information). In addition, several ECM-related proteins were identified as differentially expressed between the two conditions (Figure 1J and Table S2, Supporting Information). Interestingly, GO biological processes upregulated in a gene set enrichment analysis in pig *dECM-hyd*-cultured organoids compared to control counterparts highlighted several processes associated with vasculature and renal development, tissue remodeling, and cell-ECM interaction (Figure 1K). Altogether these findings suggested a potential role of *dECM-hyd* in facilitating kidney organoid differentiation and promoting the induction of an endogenous vascular-like cell component.

Moreover, we further explored the possibility of using *dECM-hyd* in combination with other natural components including gelatin and fibrinogen to generate biocompatible hydrogel formulations with controlled rheological properties, defining culture conditions that allowed encapsulation of PIM cells (Figure S3A, Supporting Information; see Experimental Section). For this, we first developed a pre-gel formulation consisting of 5% (w/v) gelatin, 5 mg $mL^{-1}$ fibrinogen, and 0.1% (w/v) transglutaminase (TG). This formulation was assessed based on PIM cell survival and proliferation upon encapsulation into the hydrogel formulation and their ability to differentiate and form renal vesicle (RV) structures efficiently (data not shown). We then studied the flow behavior of the established hydrogel formulation, which showed an increment of shear stress or reduction of viscosity with increasing shear rate in the different tested temperatures (from 14 to 24 °C), a rheological property known as shear thinning behavior (Figure S3B, Supporting Information). Of note, the shear thinning behavior was preserved upon the addition of 0.45% (w/v) *dECM-hyd* to the hydrogel formulation in the range of temperatures and shear rates studied (Figure S3C, Supporting Information). This rheological characteristic prevents encapsulated cells from aggressive shear stresses during extrusion, a desired requirement when aiming to use cell-laden hydrogels for bioprinting purposes. We then established the optimal cell density and crosslinking conditions for the hydrogel formulation containing 0.45% (w/v) *dECM-hyd* to generate millimeter-sized hPSC-derived renal 3D constructs (Figure S3A, Supporting Information; see Experimental Section). Briefly, day 4 PIM cells were encapsulated in the *dECM-hyd*-based formulation at a cell density of 15 million cells $mL^{-1}$ of pre-gel solution at RT and then 10 µL drops were deposited on transwell inserts and allowed to thermally crosslink at 4 °C for 10 min, after which they were further crosslinked in the presence of thrombin solution for 40 min at RT. Next, the thrombin solution was removed, and cell-laden constructs were maintained in organotypic culture conditions at 37 °C and 5% $CO_2$ in Advanced RPMI medium supplemented with FGF9 until day 11 and in the absence of growth factors in subsequent days until day 20 of differentiation (Figure S3D, Supporting Information). On day 11 numerous RVs were detected inside the renal constructs (Figure S3E, Supporting Information). The status of RV differentiation was characterized for the detection of PAX2, WT1, and ECAD by immunofluorescence and confocal analysis (Figure S3F, Supporting Information). On day 20, renal constructs contained multiple nephron-like structures (Figure S3G,H, Supporting Information) that expressed markers for the different renal compartments including podocytes (PODOCIN, NEPHRIN), proximal tubule (LTL), distal tubule (ECAD) and endothelial cells (CD31), as well as the basement membrane proteins COLLAGEN IV and LAMININ (Figure S3I, Supporting Information).

### 2.3. 2D and 3D Approaches to Generate Human Kidney Organoids Using Human Kidney Extracellular Matrix-Derived Hydrogels

Human renal cortical tissues were decellularized following the same conditions as for pig kidney (**Figure 2**A,B; see Experimental Section). After a 4 day-treatment with 1% SDS, renal tissue was then rinsed with PBS supplemented with penicillin/streptomycin followed by milliQ water washes for 5 additional days. Histological and immunofluorescence analysis of human dECMs showed the preservation of the renal cortex architecture and morphology (Figure S4A, Supporting Information). Similarly, ECM-associated proteins including LAMININ and COLLAGEN IV were detected prior to and after decellularization (Figure 2C), whereas the LTL, which stains proximal tubular cells, was undetectable in the decellularized tissue indicating the absence of cellular components (Figure 2C). In addition, the quantification of DNA in decellularized matrices confirmed the removal of the cellular material (Figure 2D). Effective tissue decellularization leads to the generation of biological scaffolds exhibiting great biocompatibility and bioactivity while preserving moderate mechanical performances for supporting cells.[32] Here, to assess the biocompatibility of human dECM materials, we made use of the CAM assay (see Experimental Section). After 4 days of implantation, human dECM matrices showed similar engraftment capacity as the native tissue, showing that our

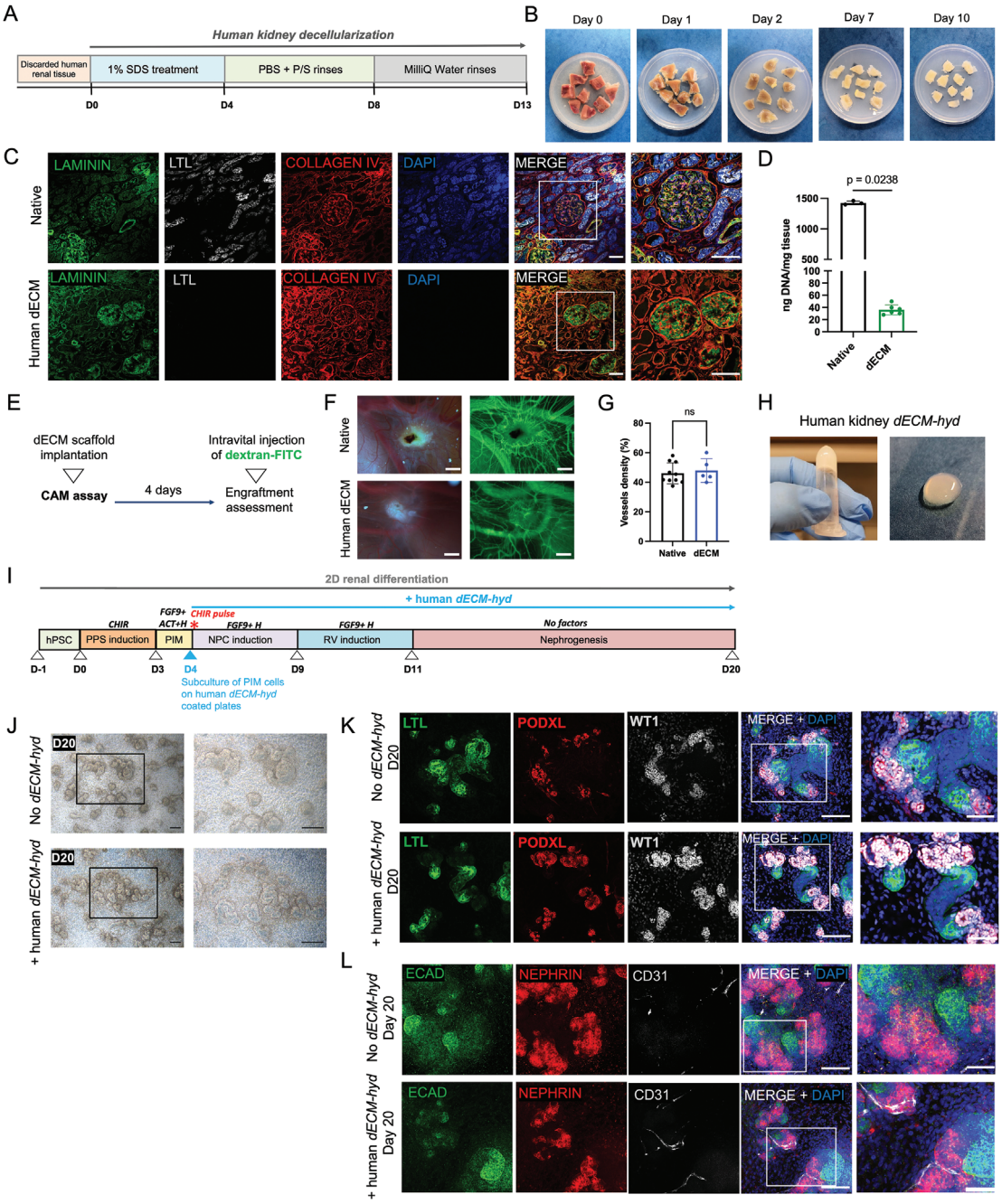


**Figure 2.** Human kidney dECM hydrogel allowed kidney organoid differentiation in 2D. A) Schematic of the protocol for human kidney decellularization. B) Representative images of human renal cortical tissue pieces during the decellularization process. Days are indicated. C) Immunohistochemical analysis of native and decellularized renal tissue for the detection of LAMININ (green), LTL (grays), COLLAGEN IV (red), and the nuclei staining DAPI (blue). Scale bars, 100 µm. D) Quantification of DNA in dECM scaffolds compared to native tissue. Data are mean ± s.d. $n = 3$ samples (native), $n = 3$ samples (dECM). Mann-Whitney test. *p*-value is indicated showing a statistically significant difference between groups. E) Schematic of the CAM assay. F) Macroscopic views of implanted native tissue and dECM scaffolds maintained *in ovo* for 4 days, and the corresponding fluorescent images obtained after intravital injection of dextran-FITC through the chick vasculature. Scale bars, 500 µm. G) Quantification of vessel density (%) in implanted native tissue and dECM scaffolds. Data are mean ± s.d. $n = 10$ samples (native), $n = 5$ samples (dECM), not significant (ns). Mann-Whitney test. H) Representative images of the human *dECM-hyd* resulting from gelation of the pre-gel at 37 °C. I) Experimental scheme for the generation of hPSC-derived kidney organoids in a 2D culture setting using human kidney *dECM-hyd* as a coating substrate and diluted in the medium from day 4 until day 20 of differentiation. J) Representative bright field images of day 20 kidney organoid structures in both tested conditions. Scale bars, 100 µm. K) Immunofluorescence analysis for the detection of LTL (green), PODXL (red), WT1 (grays), and DAPI nuclei staining (blue) in day 20 kidney organoid structures in both tested conditions. Scale bars, 100, 50 µm (magnified views). L) Immunofluorescence analysis for the detection of ECAD (green), NEPHRIN (red), CD31 (grays), and DAPI nuclei staining (blue) in day 20 kidney organoid structures in both indicated conditions. Scale bars, 100, 50 µm (magnified views). See also Figure S4, Supporting Information.

decellularization procedure allowed the preservation of major bioactivity properties including the ability to home chick embryonic vessels (Figure 2E–G and Figure S4B, Supporting Information). Deficiencies in hydrogel production from natural dECMs provide an opportunity for significant improvement to harness the full potential of dECM-based biomaterials. By optimizing key steps such as lyophilization and enzymatic digestion, it is likely to define optimal conditions to deliver dECM-derived hydrogels for applications in cell and tissue engineering. Here, to generate hydrogels, human dECM was lyophilized and enzymatically digested for 72 h at RT in acidic conditions, after which a pre-gel solution was obtained. After pH neutralization and incubation at 37 °C, the pre-gel solution was able to form a hydrogel as evaluated by the inverted tube method (Figure 2H). Next we sought to explore the angiogenic potential of human renal *dECM-hyd* to induce endogenous endothelial cell (EC) differentiation in the onset of kidney organoid differentiation in the absence of any external factor (i.e., VEGF, CHIR) compared to recent findings relaying on the addition of VEGF to generate EC-like cells.[33] To this aim, we defined a differentiation approach exploring the use of human *dECM-hyd* to induce the generation of kidney organoids in both 2D and 3D culture systems. For 2D differentiation day 4 PIM cells were enzymatically dissociated and sub-cultured into 24-well plates coated with human renal *dECM-hyd* to further promote the differentiation of PIM-like cells into NPCs through the addition of FGF9 during 7 additional days (Figure 2I). Vitronectin-coated plates were used as control counterparts. Bright field imaging and immunofluorescence analysis during the time course of renal differentiation demonstrated that the human *dECM-hyd* culture condition efficiently supported early steps of nephrogenesis in vitro in 2D through the transition of NPCs into RV structures (Figure S4C, Supporting Information) that were positively stained for PAX2 and WT1 markers (Figure S4D, Supporting Information). Under these conditions, we observed that removal of FGF9 on day 11 favored the transition of RV structures into nephron-like structures (Figure 2J), which at day 20 of differentiation expressed markers for podocyte (WT1, PODXL, NEPHRIN), proximal tubule (LTL), distal nephron (ECAD), and the endothelial marker CD31 (Figure 2K,L). Overall, these findings showed that human *dECM-hyd* supports the generation of nephron-like structures from hPSCs in the newly defined 2D conditions.

For 3D organoid generation, briefly, day 4 PIM cells were dissociated and aggregated into spheroids that were maintained under organotypic culture conditions using transwells. Human *dECM-hyd* was added into the cell culture media (1:40) from day 4 until day 20 of the differentiation process every other day (**Figure 3A**; see Experimental Section). This treatment effectively resulted in the induction of numerous RVs (Figure 3B and Figure S5A, Supporting Information) on day 11 which positively stained for PAX2, WT1, and LHX1 (Figure 3C). Upon the removal of FGF9, RVs spontaneously patterned and segmented into typical nephron-like components, including tubules (ECAD+), glomeruli (NEPHRIN+), and ECs (CD31+) by day 20 of differentiation (Figure 3D). To expand our differentiation approach to high-throughput applications, the 3D differentiation was also performed on a 96 multi-well format in floating conditions which led to similar results (Figure S5B–E, Supporting Information). Furthermore, we performed bulk RNAseq in day 20 human *dECM-hyd*-cultured organoids and found that the GO biological processes upregulated in a gene set enrichment analysis in human *dECM-hyd*-cultured organoids compared to pig *dECM-hyd*-cultured counterparts were mainly involved in endothelial development, vasculogenesis, vessel morphogenesis, connective tissue, and mesenchymal differentiation (Figure 3E). All in all, this experimental design allowed us to assess, for the first time, the utility of human renal *dECM-hyd* to support the generation of hPSC-derived nephron-like structures in 2D and 3D culture systems.

### 2.4. Engineering Kidney Organoid Vascularization through the Assembly of hPSC-Derived Endothelial Cell Spheroids and Kidney Organoids in 3D

The vasculature is a critical component in all organs, with essential functions in physiology and disease. During development, the embryonic kidney largely depends on the biochemical signaling from adjoining vasculature.[34] In this regard, ECs are being described to be minimal in kidney organoids grown in vitro.[35,36] Recently, modified protocols emphasizing shorter exposure to CHIR[37] or exogenous addition of VEGF[38] showed the generation of increased endothelial component in vitro. However, none of these elegant approaches sufficed for the incorporation of ECs into the developing glomerular-like structures. In this regard, we have recently described the transplantation of kidney organoids in the chick CAM as a new approach to promote the vascularization of developing glomeruli. That approach efficiently induced the organization and assembly of kidney organoid-resident ECs into the developing glomerular-like structures.[13]

With the aim to enrich the endogenous EC compartment in kidney organoids, we first established a protocol to generate vascular progenitors from hPSCs in 3D (**Figure 4A**; see Experimental Section). This stepwise procedure consisted of a first phase of mesoderm induction through the exposure of hPSC monolayers to 8 µM CHIR and BMP4 for 3 days, followed by subsequent specification of vascular progenitors by supplementation of the media with VEGF-A for 1 day (until day 4). On day 4, monolayers were dissociated, resuspended in medium supplemented with VEGF-A, FGF2, and 2.5% (v/v) Matrigel, and subsequently forced to aggregate into spheroids by centrifuging $10^5$ cells well$^{-1}$ of a low-adherence V-bottom 96-well plates (Figure 4A). Cell spheroids were then maintained in floating culture until day 15. Day 15 spheroids showed the formation of a network of cells expressing the endothelial marker CD31 (Figure 4B). In addition, day 7 endothelial progenitor spheroids cultured in a collagen-I:growth factor reduced (GFR) matrigel hydrogel showed the capacity to extend angiogenic-like sprouts as observed by optical microscopy, further confirming the tubulogenic capacity of the resulting hPSC-endothelial progenitors (Figure 4C). qPCR analysis during the time course of endothelial differentiation showed that from day 7 there was an increase in the expression of markers typical of an endothelial signature including KDR, CD34, VEGFR, CD31, ENDOGLIN, VEGFb, PDFGRa, and VE-CAD (Figure 4D and Figure S6A, Supporting Information). In addition, we reproducibly generated endothelial-like spheroids using an additional hPSC line (Figure S6B, Supporting Information).

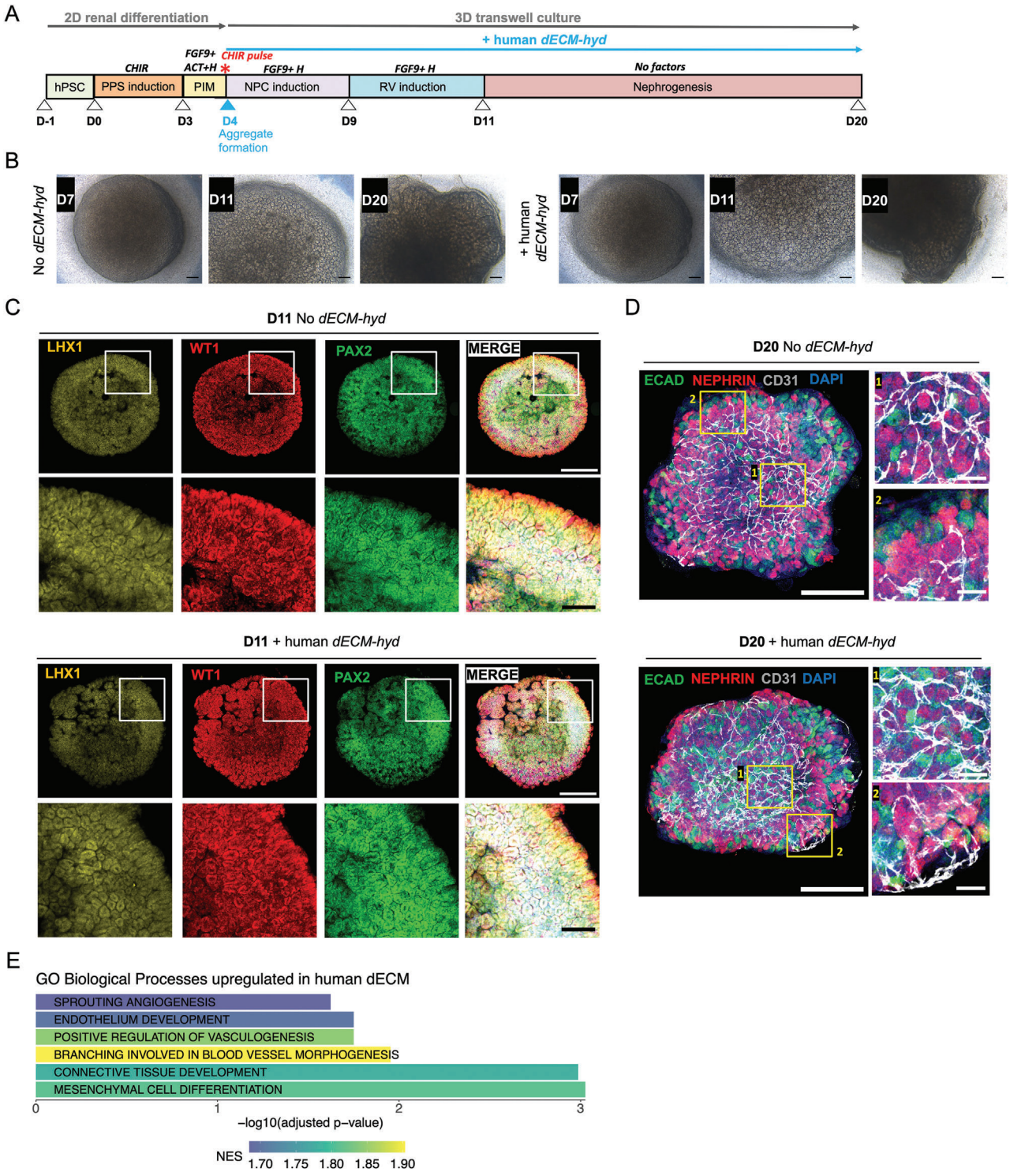


**Figure 3.** Human kidney dECM hydrogel enhanced the endothelial cell compartment in kidney organoids. A) Experimental scheme for the generation of hPSC-derived kidney organoids with human kidney *dECM-hyd* diluted in the medium from day 4 until day 20 of differentiation in a 3D transwell culture setting. B) Representative bright field images during kidney organoid generation in the presence (+human *dECM-hyd*) or absence (No *dECM-hyd*) of human *dECM-hyd*. Scale bars, 100 µm. C) Immunofluorescence analysis for the detection of PAX2 (green), WT1 (red), LHX1 (yellow), and DAPI nuclei staining (blue) in day 11 kidney organoids in both tested conditions. Scale bars, 500, 125 µm (magnified views). D) Immunofluorescence analysis for the detection of ECAD (green), NEPHRIN (red), CD31 (grays), and DAPI nuclei staining (blue) in day-20 kidney organoids in both tested conditions. Scale bars, 500, 75 µm (magnified views). E) Bar plot representing a selection of significant GO Biological processes upregulated in a gene set enrichment analysis in +human dECM-hyd cultured organoids compared to +pig dECM-hyd cultured counterparts. Bars are colored by normalized enrichment score (NES) value. See also Figure S5, Supporting Information.

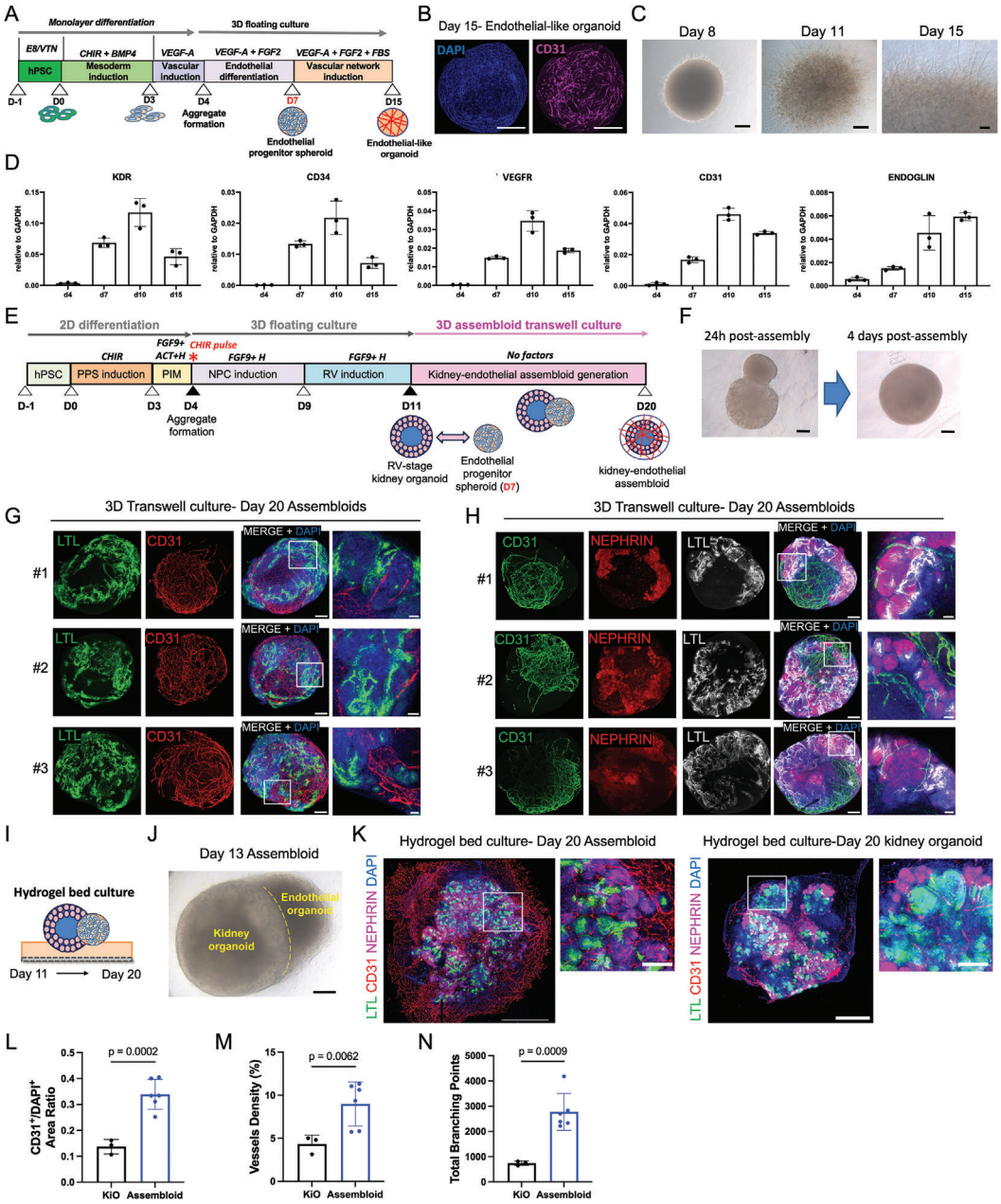


**Figure 4.** Assembly of kidney organoids with endothelial progenitor spheroids to induce vascularization. A) Schematics for the generation of endothelial organoids from hPSCs. B) Immunofluorescence and confocal analysis of a day 15 endothelial organoid for the expression of CD31 (magenta) and DAPI nuclei staining (blue). Scale bars, 200 µm. C) Representative bright field images of endothelial progenitor spheroids showing tubulogenic capacity when embedded in GFR-matrigel:collagen I for 8 days. Scale bars, 200 µm (day 8 and 11), 50 µm (day 15). D) qPCR analysis during hPSC endothelial differentiation. Genes are indicated. Data are mean ± s.d. (three technical replicates), $n = 1$ biological sample per time point. Each biological sample is a pool of 12 organoids. E) Schematics for the generation of kidney-endothelial assembloids from hPSCs. F) Representative bright field images of an assembloid 24 h and 4 days post-assembling. Scale bars, 100 µm. G) Immunofluorescence and confocal analysis of day 20 assembloids generated in transwell culture for the detection of LTL (green), CD31 (red), and DAPI nuclei staining (blue). Scale bars, 200, 50 µm (magnified views). $n = 3$ assembloids. H) Immunofluorescence and confocal analysis of day-20 assembloids generated in transwell culture for the detection of CD31 (green), NEPHRIN (red), LTL (grays), and DAPI nuclei staining (blue). Scale bars, 200, 50 µm (magnified views). $n = 3$ assembloids. I) Schematics for the hydrogel bed culture system used for assembloid differentiation from day 11 until day 20. J) Representative bright field image of a day 13 assembloid generated using the hydrogel bed culture system. Scale bar, 200 µm. K) Immunofluorescence and confocal analysis of representative day 20 assembloid and kidney organoid generated under hydrogel bed culture for the detection of LTL (green), CD31 (red), NEPHRIN (magenta), and DAPI nuclei staining (blue). Scale bars, 1000, 125 µm (magnified views). Quantification of CD31 area relative to L) DAPI, M) vessel density, and N) total branching points, in CD31 immunolabeled assembloids compared to kidney organoids (kio). For (L–N), data are mean ± s.d. $n = 3$ kidney organoid, $n = 6$ assembloids. Unpaired student's *t*-test with Whelch's correction. *p*-values are indicated showing statistically significant difference between groups. Correspondent confocal images are shown in (K) and Figure S7, Supporting Information. See also Figures S6 and S7, Supporting Information.

During kidney development, the formation of the glomerular vasculature relies on the angioblasts present in the metanephric mesenchyme which invade the capillary cleft of developing RV at the comma and S-shape stages in response to secreted cues from primitive podocytes.[39] To investigate the optimal time to incorporate our hPSC-derived vascular progenitor cells into the kidney organoids, we next determined the expression levels of endothelial-associated markers at different time points during kidney organoid development by qPCR. Endothelial-associated markers including HEY1, VEGFb, and PDGFRa started to be expressed from day 8, whereas VEGFR, VE-CAD, and ENDOGLIN were upregulated from day 15 of renal differentiation (Figure S6C, Supporting Information). Overall, these results suggested that the endogenous endothelial differentiation program in kidney organoids was active between days 8 and 15 during renal differentiation. Therefore, we decided to assembly day 7 vascular progenitor spheroids with kidney organoids at the RV-stage (day 11 of renal differentiation) (Figure 4E; see Experimental Section). For that, day 7-endothelial-like spheroids and day 11-RV-stage organoids were co-cultured in a V-bottom 96-well plate by placing one organoid of each type in each well and culturing them in endothelial and renal differentiation media at 1:1 ratio for 24 h. After 24 h (day 11 + 1), endothelial spheroids effectively fused with the RV-stage organoids (Figure 4F), resulting in assembled organoids that we called kidney-endothelial assembloids (from now on assembloids). On day 11 + 1, assembloids were transferred to organotypic culture conditions using transwells and further maintained in advanced RPMI medium in the absence of any additional factor until day 11 + 9 (day 20). Under these conditions, we found that day 20 assembloids exhibited the development of segmented nephron-like structures containing proximal tubules stained with LTL and podocyte-like cells expressing NEPHRIN, and the generation of an extensive vascular network-like structures expressing CD31 (Figure 4G,H). Importantly, this vascular component was distributed in the peritubular space close to tubule structures (Figure 4G) and in close association with glomeruli-like structures (Figure 4H). In addition, we adapted this approach to a free-floating culture system that resulted into similar results (Figure S6D,E, Supporting Information). Day 20 assembloids maintained in free-floating conditions showed expression of endothelial-associated markers (ENDOGLIN, CD31, KDR, VEGFR, VE-CAD, PDGFRa, CD34) when compared to kidney organoids as analyzed by qPCR (Figure S6F, Supporting Information). Interestingly, the mRNA levels of the proximal tubule marker SLC3A1 and the podocyte markers WT1 and SYNPO were also detected in assembloids in comparison to kidney organoids (Figure S6F, Supporting Information), suggesting that the incorporation of a vascular-like component in developing kidney organoids allows for the generation of nephron-like structures. We have previously shown that soft substrate environments promoted the development of more nephron-like structures with enhanced maturation-associated features.[13] Following this rationale, we hypothesized that soft hydrogel substrates might enhance the self-organization ability of endothelial progenitors into the assembloids, further promoting renal differentiation. In light of our observations, we next explored the possibility to combine commercially available natural materials such as collagen-I and GFR-matrigel to formulate a hydrogel substrate that could serve as an extracellular matrix surrogate for assembloid differentiation from hPSCs. Indeed, these natural components have been largely used in different in vitro models to study cancer cell migration dynamics,[40] or the formation of vessel-like structures from human endothelial cell lines,[41] among others. In view of all these observations, we formulated a combined hydrogel at 3:1 volume ratio of collagen I at 2 mg $mL^{-1}$ to GFR-matrigel and conducted oscillatory rheology (see Experimental Section) as prior works have shown that the rheological properties of 3D environments are extremely relevant for organoid culture.[10,42] We observed a pre-gel viscous behavior of the material before reaching 25 °C, indicated by the presence of both storage (G´) and loss (G´´) moduli (Figure S7A,B, Supporting Information). At this stage, the storage modulus (reflecting the solid-like behavior) remained lower than the loss modulus (indicating liquid-like behavior), with G´< G´´, suggesting a pre-gel state (Figure S7A,B, Supporting Information). Gelation occurred around 26–28 °C, evidenced by the shift to G´> G´´, which indicated the temperature dependence of gelation in the material (Figure S7B, Supporting Information). This transition from pre-gel to gel state took place approximately after 21 min of measurement (Figure S7A, Supporting Information). Following gelation, both moduli reached a plateau after about 60 min (Figure S7A, Supporting Information), indicating complete gelation. Next, we generated kidney-endothelial assembloids onto the collagen-I:GFR-matrigel hydrogel using the transwell culture system, referred to here as hydrogel bed culture system. By co-culturing a day 7- endothelial spheroid in contact with a day 11 RV-stage organoid using the hydrogel bed culture system (Figure 4I; see Experimental Section), we observed that readily after 2 days the endothelial spheroid completely fused with the renal organoid forming the so-called 3D assembloid (Figure 4J). Under these conditions and in the absence of any additional growth factor, assembloids were allowed to grow and differentiate for 7 additional days. As analyzed by immunofluorescence and confocal imaging, day 20 assembloids showed the presence of vascular-like structures characterized by CD31 expression, and the presence of numerous nephron-like structures that were infiltrated with vessel-like structures (Figure 4K). Notably, CD31+ capillary-like structures were in close contact with the NEPHRIN+ podocyte-like cells and surrounded the LTL+ proximal tubule-like structures (Figure 4K, magnified view). Image analysis quantification showed that day 20 assembloids possessed an enhanced CD31+ EC compartment compared to kidney organoids (Figure 4K,L and Figure S7C, Supporting Information), as well as increased CD31+ vessel density (Figure 4M) and total branching points (Figure 4N). Overall, our approach allowed the generation of vascular progenitors from hPSCs that, upon 3D co-culture with RV-stage kidney organoids, showed the ability to self-organize into vascular-like structures while sustaining the development of segmented nephron-like structures in the resulting assembloids.

## 3. Outlook

The impact of natural-derived hydrogels has been largely studied on different types of stem cells, but fewer reports exist on their effects on aggregates and organoids. Similarly, the potential effect of these natural hydrogels on complex processes such as stem cell differentiation and vascularization remain largely

unexplored. Here we have revised several steps allowing for the generation of porcine and human kidney dECM-derived hydrogels which were further engineered to establish different culture conditions in 2D and 3D supporting renal differentiation from hPSCs. Our observations indicate that natural-derived hydrogels had a direct impact on the extent of kidney organoid differentiation as shown using bulk RNA sequencing and further analysis including immunofluorescence and image analysis quantification. With the aim to extend the potential applications of our results, we further investigated the impact of these hydrogels on the promotion of endogenous vascularization within the time course of kidney organoid differentiation, observing that these biomaterials support the formation of cells of the vascular lineage. In light of these results, we proceeded to define a new approach supporting the assembly of developing kidney organoids with endothelial organoids to promote the vascularization of different kidney compartments, including tubular- and glomerular-like structures. Overall, our results show the potential advantages of natural-derived hydrogel properties to externally control the extent of differentiation and vascularization of the resulting kidney organoids. Further understanding of how to properly engineer natural hydrogels will be important to define robust and well-defined conditions to generate functional engraftments and to establish platforms for disease modeling applications replicating complex pathological scenarios influenced by vascular malfunction, as diabetic nephropathy.

## 4. Experimental Section

*Decellularization of Kidney Tissues*: Porcine kidneys were harvested from adult healthy pigs (strain hybrid landrace/large white crossbreed) under general anesthesia. All animal care and procedures followed guidelines by the European Union (directive 2010/63/EU) and local regulations. Human renal tissue was obtained from healthy renal tissues after nephrectomy of renal cell carcinomas. The experimental procedure was approved by the Guarantee Commission for the Donation and Use of Human Cells and Tissues and the Clinical Research Ethics P-CMR[C]/IDIBELL, and the ethics committee from the Hospital Clinic de Barcelona (project no. 0336/13304/2019). Kidney tissues were preserved at −80 °C until further use.

For decellularization, frozen renal tissues were thawed on ice overnight. Renal cortex was separated from the medulla manually and tissue samples were then minced into small pieces that were placed in an sterile glass recipient and rinsed several times with PBS supplemented with penicillin/streptomycin (penicillin 10 000 U $mL^{-1}$:streptomycin 10 000 µg $mL^{-1}$; 15140122, Life Technologies) and milliQ water while maintained under constant agitation to remove the remaining blood and generate hypotonic cell lysis. The washes were performed until the solution had a transparent appearance. Next, renal cortex slices were decellularized by immersion into 1% sodium dodecyl sulfate (SDS;161-0301, Bio-Rad, Sigma) in deionized water while shaking for 4 days with solution changes every 2 h during the first 2 days and twice a day thereafter. Next, samples were rinsed thoroughly with PBS containing antibiotics for 4 additional days, and finally with milliQ water for another 5 days.

*DNA Quantification*: Genomic DNA was isolated from native kidney and dECM samples using the DNeasy Blood & Tissue Kit (69506, Qiagen) following the manufacturer's instructions. DNA samples were then quantified by spectrophotometry (Nanodrop, ND-100, Spectrophotometer).

*Collagen Quantification*: The acid-/pepsin-soluble collagen content in kidney dECMs and pre-gel samples was measured using a Sircol soluble collagen assay kit (S1000, Biocolor life science assays) following the manufacturer's instructions. Briefly, samples were mixed with Sircol Dye Reagent and incubated for 30 min under constant agitation to induce the binding of the dye to collagen. After centrifugation, collagen-bound dye pellets were washed with ice-cold Acid-Salt Wash Reagent to remove the unbound dye. Next, samples were centrifuged, and pellets were resuspended in Alkali Reagent to release the collagen bound dye. After incubation, the relative absorbance was measured at 540 nm using a 96-well plate using a Benchmark Plus Microplate Reader (BIO-RAD). A reagent blank and a set of collagen standards were used as references to determine the collagen concentration of the tested samples.

*Elastin Quantification*: The soluble elastin content in the kidney dECM scaffolds and pre-gel solutions was measured using the Fastin elastin assay kit (F2000, Biocolor life science assays). Samples were mixed with Elastin Precipitating Reagent and incubated for 15 min to induce elastin precipitation. Next, samples were centrifuged, and elastin precipitates were mixed with Dye Reagent and incubated for 90 min under constant agitation to induce the reaction between the dye and the $\alpha$-elastin. Finally, the elastin-dye pellets were mixed with dye dissociation reagent to induce the release of the elastin bound dye. After 10 min of incubation, the absorbance was measured in a 96-well plate at 513 nm using a Benchmark Plus Microplate Reader (BIO-RAD). A reagent blank and a set of $\alpha$-elastin standards were used as references to determine the elastin content of the tested samples.

*Preparation of Kidney dECM Pre-Gel Solution*: dECM were frozen at −80 °C for 24 h and subsequently lyophilized for 48 h. Samples were manually milled into small pieces and solubilized using pepsin (P6887, Sigma) in 0.1N hydrochloric acid pH 1 (258148, Sigma) in a ratio 1:10 (pepsin: dECM) in agitation at RT for 72 h under constant shaking. Next, the pH of the dECM solution was adjusted with dropwise addition of cold 1 M NaOH solution while maintaining the solution on ice to avoid gelation. The pH-adjusted dECM pre-gel solution was aliquoted and stored at −20 °C for further use. To allow gel formation, the neutralized pre-gel solution was incubated at 37 °C for 1 to 2 h.

*Inverted Tube Method*: Gelation tests were performed by adding 0.5 mL of salt- and PH-adjusted pre-gel in a 2 mL Eppendorf vial and incubating it at 37 °C for 1 to 2 h. Gelation was considered to have occurred when a solid-like material was obtained that did not exhibit gravitational flow (inverted test tube method) during a period of 5 min.

*Scanning Electron Microscopy*: *dECM-hyd* samples were fixed in a 0.1 M phosphate buffer containing 2.5% glutaraldehyde (G7776, Sigma Aldrich) overnight at 4 °C. Subsequently, they were fixed in 1% osmium tetroxide (Sigma) for 2 h, dehydrated through a graded ethanol-water series solutions (from 50% to 100%) (v/v). All samples were critical point dried, sputter-coated with gold in a Polaron E 5100 coating apparatus (Quorum technologies, Lewis, UK), and observed under JSM-840A SEM (JEOL, Tokyo, Japan).

*Chick Chorioallantoic Membrane Assay (CAM)*: Following animal care guidelines in Spain, no approval was required to perform the experiments described here. Native and decellularized matrices and derived hydrogels were implanted into the CAM following the previously published methodology.[13] Briefly, fertilized white Leghorn chicken eggs were supplied by Granja Gibert. After 24 h, 3 mL of albumin was extracted from the egg using an 18-gauge syringe. At embryonic day 7 (ED 7), the chick CAM was exposed by cutting a window (2 $cm^2$) on the eggshell. Biomaterials were placed on the CAM by gently scraping the upper CAM layer (avoiding bleeding or visible rupture of capillaries) and the window in the shell was sealed with adhesive tape. Eggs were incubated for 4 additional days (ED 11). Representative CAMs from each experimental group were imaged using a using an MZ10 F Leica stereomicroscope equipped with an MC170 HD Leica camera. The number of fine distinct blood vessel branch points was counted. Angiogenesis was assessed by the sprouting of new vessels from preexisting vessels in response to *dECM hyd*. The angiogenic index was determined using WimCAM software (Wimasis) that measures total vessel network length, vessel density, vessel branching points, total segments, and mean segment length. At least 2 chick embryos were used per group.

*Intravital Imaging of the CAM Vasculature*: Under a dissecting microscope, superficial CAM veins were injected with 1 mg $mL^{-1}$ FITC-dextran (2 MDa) (FD-2000S, Sigma) in PBS using a 30-gauge Hamilton syringe, allowing solutions to circulate for 5 min. Injected volumes were kept at

50 µL. Live imaging was performed using an MZ10 F Leica stereomicroscope equipped with an MC170 HD Leica camera.

*Culture of hPSCs*: hPSC lines were obtained after the approval of the Ethics Committee of the Center of Regenerative Medicine in Barcelona and the Comisión de Seguimiento y Control de la Donación de Células y Tejidos Humanos del Instituto de Salud Carlos III (project numbers: 0336/2723/2021; 0336/1123/2021; 0336/214/2022). hESC ES[4] line and CBiPS1sv-4F-40 iPSC line were obtained from The National Bank of Stem Cells (ISCIII, Madrid). Both hPSC lines were maintained and grown in Essential 8 medium (A1517001, Life Technologies) in cell culture plates coated with 5 µg $mL^{-1}$ vitronectin (A14700, Fisher Scientific) with 5% CO2 at 37 °C. Cells were passaged every 4–6 days by disaggregating hPSC colonies into small cell clusters using 0.5 mM EDTA (E9884, Sigma).

*hPSC Differentiation into Renal Progenitor Cells*: hPSCs were differentiated into PIM-committed cells following the recently published differentiation protocol.[13] Briefly, hPSCs were first dissociated using 0.5 mM EDTA (E9884, Sigma) and seeded at a final density of $5 \times 10^4$ cells $cm^{-2}$ onto vitronectin-coated plates in the presence of Essential 8 (E8) medium (day -1 of the differentiation protocol). Next day, E8 media was changed and differentiation was initiated by treating hPSCs with advanced RPMI 1640 basal medium (12633-012, Life Technologies) supplemented with 8 µM CHIR (SML1046, Sigma), 2 mM L-GlutaMAX (35050-038, Life Technologies) in the presence of penicillin/streptomycin (penicillin 10 000 U $mL^{-1}$:streptomycin 10 000 µg $mL^{-1}$; 15140122, Life Technologies). Media changes were performed every day for 3 consecutive days (from days 0 to 3 of the differentiation protocol) to induce the derivation of posterior primitive streak committed cells. Next, cell cultures were treated with 200 ng $mL^{-1}$ FGF9 (100-23B, Peprotech), 1 µg $mL^{-1}$ heparin (H3149-10KU, Sigma), and 10 ng $mL^{-1}$ activin A (338-AC-050, Vitro) for one additional day to generate PIM committed cells (from days 3 to 4 of the differentiation protocol). On day 4 of the differentiation process PIM cell monolayers received a single pulse of 5 µM CHIR during 1 h in the presence of advanced RPMI 1640 basal medium supplemented with 2 mM L-GlutaMAX and penicillin/streptomycin, 200 ng $mL^{-1}$ FGF9 and 1 µg $mL^{-1}$ heparin. After 1 h cell monolayers were detached softly using TrypLE Express Enzyme (1260402, ThermoFisher) for 1 min, collected, and counted. PIM-committed cell suspensions were used for kidney organoid generation in 2D and 3D culture settings in the presence or absence of *dECM-hyd*.

*hPSC Differentiation into Kidney Organoids in 2D and 3D Culture Settings*: In the 2D culture setting, day 4 PIM-committed cell suspensions, obtained after the 5 µM CHIR-pulse and subsequent dissociation of the monolayer, were seeded at 1.5–2.5 × $10^5$ viable cells $well^{-1}$ on 24 multi-well plates coated with 0.075% w/v of *dECM-hyd* (1:40 dilution) or 5 µg $mL^{-1}$ vitronectin (as control counterpart) in advanced RPMI 1640 basal medium supplemented with 2 mM L-GlutaMAX and penicillin/streptomycin, 200 ng $mL^{-1}$ FGF9 and 1 µg $mL^{-1}$ heparin. In the 3D setting, day 4 PIM-committed cell suspensions were seeded to achieve $10^5$ cells per well on V-shape 96 multi-well plates (249935, ThermoFisher) in advanced RPMI 1640 basal medium supplemented with 2 mM L-GlutaMAX, penicillin/streptomycin, 200 ng $mL^{-1}$ FGF9, 1 µg $mL^{-1}$ heparin and 1:40 dilution (0075% w/v) of *dECM-hyd*, and centrifuged at 300 g for 5 min to form one aggregate per well. Control counterparts (No *dECM-hyd*) were cultured without the addition of *dECM-hyd* in the medium. In both 2D and 3D culture settings, monolayers or organoids were cultured for 7 days (from days 4 to 11 of the differentiation process) in advanced RPMI 1640 basal medium supplemented with 200 ng $mL^{-1}$ FGF9 and 1 µg $mL^{-1}$ heparin, changing the medium every other day. On day 11, factors were removed, and organoids were maintained in advanced RPMI 1640 basal medium until day 20 of differentiation changing the medium every third day. *dECM-hyd* was refreshed in the medium at 1:40 dilution (0075% w/v) in each medium change. For 3D floating culture, organoids were maintained in V-shape 96 multi-well plates during the entire differentiation period. For 3D transwell culture day 6 organoids were transferred to transwell inserts (CLS3460, Sigma) and cultured in air-liquid interphase until day 20.

*Preparation of Hydrogel Formulations to Generate Renal Constructs*: The composite pre-gel was a mixture of 5% (w/v) gelatin (G1890, Sigma), 5 mg $mL^{-1}$ fibrinogen (F8630, Sigma), 0.1% (w/v) transglutaminase (TG) (BDF PROBINDR) and 0.45% (w/v) *dECM-hyd*. Briefly, gelatin and fibrinogen solutions, and *dECM-hyd* were mixed at RT until homogeneous to achieve the indicted final concentrations. At this moment, TG solution was added and thoroughly mixed. For cell encapsulation, day 4-PIM-committed cells were gently combined with pre-gel solution immediately after the addition of the TG to achieve a final cell density of 15 million cells $mL^{-1}$. Then, 5 to 10 µL drops of the cell-laden pre-gel were deposited on transwell inserts (CLS3460, Sigma) and allowed to thermally crosslink at 4 °C for 10 min. The resulting cell-laden hydrogel constructs were further crosslinked in the presence of 10 U $mL^{-1}$ thrombin solution for 40 min at RT. Next, thrombin solution was removed, and cell-laden constructs were maintained at 37 °C and 5% $CO_2$ in air-liquid interphase in Advanced RPMI medium with 200 ng $mL^{-1}$ FGF9 and 1 µg $mL^{-1}$ heparin until day 11 of the renal differentiation process, and in the absence of growth factors in subsequent days until day 20 of differentiation. Medium changes were performed every other day.

*Generation of Endothelial-Like Organoids from hPSCs*: hPSCs were first dissociated using 0.5 mM EDTA (E9884, Sigma) and seeded at a final density of $5 \times 10^4$ cells $cm^{-2}$ onto vitronectin-coated plates in the presence of Essential 8 (E8) media (day 1 of the differentiation protocol). Next day, E8 media was changed and differentiation was initiated by treating hPSCs with advanced DMEM:F12 basal medium (12634010, Life Technologies) supplemented with 8 µM CHIR (SML1046, Sigma), 25 ng $mL^{-1}$ BMP4 (130-111-165, Miltenyi Biotec), 2 mM L-GlutaMAX (35050-038, Life Technologies) and penicillin/streptomycin (penicillin 10 000 U $mL^{-1}$:streptomycin 10 000 µg $mL^{-1}$; 15140122, Life Technologies). Media changes were performed every day for 3 consecutive days (from days 0 to 3 of the differentiation protocol) to induce the derivation of mesoderm committed cells. Next, cell cultures were treated with 100 ng $mL^{-1}$ VEGF-A (100-20, Peprotech) in advanced DMEM:F12 basal medium supplemented with 2 mM L-GlutaMAX and penicillin/streptomycin (penicillin 10 000 U $mL^{-1}$:streptomycin 10 000 µg $mL^{-1}$) for one additional day to induce endothelial progenitor committed cells (from days 3 to 4 of the differentiation protocol). On day 4 of the differentiation process endothelial progenitor monolayers were detached softly using TrypLE Express Enzyme (1260402, ThermoFisher) for 1 min, collected, and counted. Next, day 4 endothelial progenitor cell suspensions were seeded on V-shape 96 multi-well plates (249935, ThermoFisher) and centrifuged at 300 g for 5 min to form one cell aggregate per well in advanced DMEM:F12 basal medium supplemented with 100 ng $mL^{-1}$ VEGF-A, 100 ng $mL^{-1}$ FGF2 (130-093-841, Miltenyi Biotec), 2 mM L-GlutaMAX, penicillin/streptomycin (penicillin 10 000 U $mL^{-1}$:streptomycin 10 000 µg $mL^{-1}$). Organoids were cultured from days 4 to 7 in the presence of 100 ng $mL^{-1}$ VEGF-A, 100 ng $mL^{-1}$ FGF2, changing the medium every other day. Medium was also supplemented with 2.5% (v/v) growth factor reduced (GFR) Matrigel (45356231, Corning) from day 4 until day 6 of differentiation. On day 7, medium was changed to advanced DMEM:F12 basal medium supplemented with 100 ng $mL^{-1}$ VEGF-A, 100 ng $mL^{-1}$ FGF2, 2 mM L-GlutaMAX, penicillin/streptomycin (penicillin 10 000 U $mL^{-1}$:streptomycin 10 000 µg $mL^{-1}$) and 10% FBS (Gibco) to induce the formation of endothelial cell network-like structures, changing the medium every third day until day 15 of the differentiation process. For testing the tubulogenic capacity of day 7 endothelial progenitor spheroids, they were embedded in Collagen I (5005, PureCol Type I Collagen, Cell Systems):GFR-matrigel (45356231, Corning) (3:1) hydrogel and maintained in advanced DMEM:F12 basal medium supplemented with 100 ng $mL^{-1}$ VEGF-A, 100 ng $mL^{-1}$ FGF2, 2 mM L-GlutaMAX, penicillin/streptomycin (penicillin 10 000 U $mL^{-1}$:streptomycin 10 000 µg $mL^{-1}$) and 10% FBS (Gibco) for at least 4 days.

*Generation of Kidney-Endothelial Assembloids from hPSCs*: Day 7-endothelial-like spheroids derived from hPSCs were assembled with day 11-RV-stage kidney organoids by co-culturing one endothelial-like spheroid with one RV-stage kidney organoids in each well of a V-bottom 96-well plate and maintained in 1:1 ratio of endothelial differentiation medium (advanced DMEM:F12 basal with 100 ng $mL^{-1}$ VEGF-A, 100 ng $mL^{-1}$ FGF2, 2 mM L-GlutaMAX, and penicillin/streptomycin) and kidney differentiation medium (advanced RPMI 1640 basal medium with 2 mM L-GlutaMAX and penicillin/streptomycin) for 24 h. After 24 h (on day 11 + 1), assembled organoids, referred as to assembloids, were maintained

in 3D floating conditions, or transferred to transwell inserts in air-liquid interphase culture in advanced RPMI 1640 basal medium with 2 mM L-GlutaMAX and penicillin/streptomycin without the addition of any other factor until day 11 + 9 (day 20) of differentiation. For hydrogel bed culture, after 2h-assembly of day 7-endothelial spheroids with day 11-RV-stage kidney organoids, the resulting assembloids were carefully transferred to transwell inserts coated with a soft hydrogel bed composed of Collagen I at 2 mg $mL^{-1}$ (5005, PureCol Type I Collagen, Cell Systems):GFR-matrigel (45356231, Corning) (3:1) and cultured in the air-liquid interphase in advanced RPMI 1640 basal medium with 2 mM sL-GlutaMAX and penicillin/streptomycin without the addition of any other factor until day 11 + 9 (day 20) of differentiation.

*Rheological Characterization of Hydrogels*: The rheological properties of the gelatin/fibrinogen/TG hydrogel mixtures with or without supplementation of 0.45% (w/v) of pig dECM were characterized with a rheometer MCR 702 Multidrive in controlled shear stress mode, equipped with a steel cone geometry of 1° and 40 mm (CP40-1). Flow ramps to obtain shear stress versus shear rate and viscosity versus shear rate were performed from 100 to 0.01 $s^{-1}$, in logarithmic mode with 600 s of duration per point, with a pre-conditioning of 30 s and a pre-shear of 3 rad $s^{-1}$ for 10 s. The rheological properties of the collagen-I:GFR-matrigel combined hydrogel used in the assembloid experiments were characterized in an Anton Paar rheometer MCR702. Briefly, 350 µL of pH-neutralized hydrogel was transferred into a thermostatic Peltier unit of the rheometer. This was coupled with a cone plate of 39.953 mm diameter, specifically CP40-1, no 2627, with a fixed working gap of 0.078 mm. Measurements were conducted in triplicate ($n = 3$), initiating with a constant temperature ramp from 4 to 37 °C over 30 min (1.1 °C $min^{-1}$), followed by a 70-min duration at 37 °C. Oscillation tests, determining the storage and loss modulus, were performed at a constant oscillating shear strain of 0.1% and a constant angular frequency of 10 rad $s^{-1}$ for 100 min. Data processing utilized Anton Paar RheoCompass software (v.1.32), and GraphPad Prism software (v.10).

*Histology and Immunocytochemistry*: Native and decellularized renal cortex slices were fixed with 4% paraformaldehyde (153799, Aname) overnight at 4 °C. Samples were then washed twice with PBS, embedded in paraffin blocks, and sectioned into 5 to 10 µm samples. Sections were stained for Hematoxylin and Eosin, Periodic acid-Schiff (PAS), Masson's trichrome, and Verhoeff's elastic stain (VEG). Images were captured using a Leica light microscope. For immunofluorescence, samples were fixed with 4% paraformaldehyde (153799, Aname) overnight at 4 °C, washed twice with PBS, and blocked using Tris-buffered saline (TBS) containing 6% donkey serum (S30, Millipore) and 1% Triton X-100 (T8787, Sigma) for 1 h at room temperature. Next, samples were treated overnight at 4 °C with the indicated primary antibodies (Table S3, Supporting Information) diluted in antibody dilution buffer (TBS solution with 6% donkey serum and 0.5% Triton X-100). After incubation with primary antibodies samples were then washed three times with antibody dilution buffer and further incubated for 4 h at room temperature with fluorescent conjugated secondary antibodies (Alexa Fluor (A) 488-, Cy3- or A647-; 1:200) (Table S4, Supporting Information). For LTL detection samples were stained for biotinylated LTL (B-1325, Vector Labs) using a streptavidin/biotin blocking kit (SP-2002, Vector Labs). Detection of LTL+ cells was made using Alexa Fluor 488 conjugated with streptavidin (SA5488, Vector Labs). Nuclei were stained using 4,6-diamidino-2- phenylindole (DAPI; 1:5000, D1306, Life Technologies) for 30 min. The samples were then mounted in Fluoromount-G (0100-01, Southern Biotech) and visualized using the SP5 Leica microscope, a Zeiss LSM780 or LSM 880-Airyscan Elyra confocal microscope, or a Nikon LIPSI – Spinning Disk confocal HCS/HTS microscope.

*Total RNA Isolation and qPCR with Reverse Transcription*: Isolation of total RNA was performed using Tri-Reagent following the manufacturer's recommendations (T9424 Sigma). All samples were treated with TURBO DNase inhibitor (Ambion AM1907) to remove any residual genomic DNA: Then 1ug of RNA was retrotranscribed to cDNA using iScript cDNA Synthesis kit (12328, Invitrogen). cDNAs (25 ng $well^{-1}$) were used for gene expression quantification for the indicated primers (Table S5, Supporting Information) in the presence of the PowerUp Syber Green Master Mix (A25742, Thermo Fisher Scientific) using Quantitative PCR QUANSTUDIO 5 (2Applied Biosystems, Thermo Fisher Scientific).

*Bulk RNA-Sequencing*: Roughly between 100 and 150 ng of total RNA were used for transcriptomic interrogation of kidney organoids in different culture conditions using Illumina Stranded Total RNA Prep Ligation with Ribo-Zero Plus according to the manufacturer's instructions. Briefly, cytoplasmic and mitochondrial rRNAs as well as beta globin transcripts were depleted from the samples. The remaining RNA was fragmented and reverse-transcribed. A second strand cDNA synthesis step removed the RNA template while incorporating dUTP in place of dTTP to preserve strand specificity. Next, double-stranded cDNA was A-tailed, then ligated to Illumina anchors bearing T-overhangs. PCR-amplification of the library allowed the barcoding of the samples with 10 bp dual indexes and the completion of Illumina sequences for cluster generation. Libraries were quantified with Qubit dsDNA HS Assay Kit and their profile was examined using Agilent's HS D1000 ScreenTape Assay. Sequencing was carried out in an Illumina NextSeq 2000 using paired-end, dual-index sequencing (Read1: 59 cycles; i7: 10 cycles; i5: 10 cycles Read2:59 cycles) at a depth of about 50 million reads per sample.

*Bulk RNA-Sequencing Analysis*: Samples were demultiplexed using the Illumina bcl2fastq software (v.2.2.0) and aligned to the human genome (GRCh38) with STAR (v2.7.0d) using default parameters. Gene expression quantification was performed using the featureCounts function implemented in the R package Rsubread (v2.4.3) counting uniquely mapped paired-end reads with reverse strandness. The Ensembl v93 gene annotation was considered as the reference. The filterbyExpr function implemented in the edgeR package (v3.40.2) was used to filter out genes with a low number of counts for downstream analyses. Data normalization, transformation (considering variance stabilizing transformation), principal component analysis, and differential expression analyses with the Wald test and an FDR of 0.05 were performed with the DESeq2 package (v1.38.3). Gene set enrichment analyses (GSEA) were done with the fgsea (v1.24.0) R package, considering the GO Biological Processes and ordering genes by shrunken log fold-change.

*Statistical Analysis*: All data are presented as mean ± s.d. and other details such as the number of replicates and the level of significance are mentioned in figure legends. Statistical analysis was done in GraphPad Prism software (v.9 or v.10) (GraphPad software, https://www.graphpad.com/scientific-software/prism). Mann-Whitney test and unpaired student's *t*-test with Whelch's correction were used to analyze intergroup differences. *p*-values less than 0.05 were considered statistically significant.

## Supporting Information

Supporting Information is available from the Wiley Online Library or from the author.

## Acknowledgements

The authors thank all members of the laboratories for helpful discussions and technical support. This work received funding from the European Union's Horizon 2020 and Horizon Europe Research and Innovation Programme (European Research Council (ERC) ERC CoG-2020_101002478_ENGINORG to N.M., GA- 874827 BRAV3 to N.M., A.U.-A., C.T., A.V.-Z. and F.P., GA- 964342–ECABOX to N.M. and E.G., and GA- 101057129 _REACT to N.M. and D.M.-R., and iNANOSWARMS under grant agreement No 866348 to S.S. and D.E.-U.). S.S. and D.E.-U. were also supported by MCIN/AEI/10.13039/501100011033 (PID2021-128417OB-I00) and "ERDF A way of making Europe". This project received funding from the Innovative Medicines Initiative 2 Joint Undertaking (JU) under grant agreement no. 101005026. The JU receives support from the European Union's Horizon 2020 research and innovation program and EFPIA. This work was also supported by the MCIN/AEI/10.13039/501100011033 (PID2020-119929RB-I00 to N.M.), MCIN/European Union—"Next Generation EU/PRTR" (PLEC2021-008127 to N.M., I.G., A.M.Z. and F.P.), and the Generalitat de Catalunya and CERCA Programme (2021 SGR

00760 to N.M.). This study was funded by Instituto de Salud Carlos III (ISCIII) through the Biobanks and Biomodels Platform and co-funded by the European Union (PTC20/00013 and PTC20/00130 to N.M., and PT20/00133 to A.C.) and by Instituto de Salud Carlos III and European Union—Next Generation EU, Plan de Recuperación Transformación y Resiliencia (TERAV/ISCIII RD21/0017/0018 to N.M. and A.M., RD21/0017/0002 to M.E.F.-S., and RD1/0017/0009 to F.P.). This work was supported by funds from the ISCIII Red TERCEL RETIC (RD16/0011/0005 to F.P.), and CIBERONC (CB16/12/00489 to F.P.) and co-financed by European Regional Development Fund-FEDER "A way to make Europe" and Next Generation EU, Plan de Recuperación Transformación y Resiliencia (to F.P). This work received funding from Gobierno de Navarra Departamento de Desarrollo Económico y Empresarial AGATA (0011-1411-2020-000011) and DIANA (0011-1411-2017-000029) (to F.P., A.U.-A., and A.V.-Z.). G.A. is funded through the PhD programme "Joan Oró" - Departament de Recerca i Universitats, Generalitat de Catalunya (Ref. 2023 FI-1 00800), and co-financed by the European Union (FSE). A.U.-A. was supported by a Sara Borrell grant (CD22/00027) from the Instituto Carlos III and NextGenerationEU. This work received funding from Fundació la Marató de TV3 (202125–30 to N.M.).

## Conflict of Interest

The authors declare no conflict of interest.

## Author Contributions

D.M.-R. and A.M. contributed equally to this work. This study was conceived and designed by N.M. E.G. and N.M. wrote the paper. E.G. and D.M.-R. performed all cell culture experiments and organoid data analysis including immunofluorescence, confocal image acquisition, and analysis. A.M. performed image processing and quantification. E.G., D.M.-R., and M.K. performed CAM assay experiments. E.G., D.M.-R., M.G., and M.K. performed kidney decellularization experiments and dECM characterization. D.M.-R., G.A., C.T., and M.G. performed qPCR analysis. A.C. and L.I.R. performed the harvesting of kidney tissues. M.E.F.-S. helped and supervised the establishment of decellularization procedures. D.E.-U., R.M., I.G., A.M.Z., and S.S. performed the rheological characterization of hydrogels. A.V.-Z. prepared RNA-seq samples. A.U.-A. and F.P. performed the RNA-seq data analysis on kidney organoids.

## Data Availability Statement

The data that support the findings of this study are available from the corresponding author upon reasonable request. Bulk RNA-Seq data are publicy available in Gene Expression Omnibus (GEO, http://www.ncbi.nlm.nih.gov/geo) under the accession number GSE250468.

## Keywords

assembloids, extracellular matrix-derived hydrogels, human pluripotent stem cells, kidney organoids, vascularization

Received: January 7, 2024
Revised: May 14, 2024
Published online:

[1] M. H. Little, A. P. McMahon, *Cold Spring Harbor Perspect. Biol.* **2012**, *4*, a008300.
[2] J. Liao, Z. Yu, Y. Chen, M. Bao, C. Zou, H. Zhang, D. Liu, T. Li, Q. Zhang, J. Li, J. Cheng, Z. Mo, *Sci. Data* **2020**, *7*, 4.
[3] M. D. Young, T. J. Mitchell, F. A. Vieira Braga, M. G. B. Tran, B. J. Stewart, J. R. Ferdinand, G. Collord, R. A. Botting, D. M. Popescu, K. W. Loudon, R. Vento-Tormo, E. Stephenson, A. Cagan, S. J. Farndon, C. Del, M. Velasco-Herrera, C. Guzzo, N. Richoz, L. Mamanova, T. Aho, J. N. Armitage, A. C. P. Riddick, I. Mushtaq, S. Farrell, D. Rampling, J. Nicholson, A. Filby, J. Burge, S. Lisgo, P. H. Maxwell, et al., *Science* **2018**, *361*, 594.
[4] N. Montserrat, E. Garreta, J. C. Izpisua Belmonte, *FEBS J.* **2016**, *283*, 3303.
[5] V. A. Luyckx, Z. Al-Aly, A. K. Bello, E. Bellorin-Font, R. G. Carlini, J. Fabian, G. Garcia-Garcia, A. Iyengar, M. Sekkarie, W. van Biesen, I. Ulasi, K. Yeates, S. J. Sustainable, *Nat. Rev. Nephrol.* **2021**, *17*, 15.
[6] E. F. Carney, *Nat. Rev. Nephrol.* **2020**, *16*, 251.
[7] E. Garreta, F. González, N. Montserrat, *Nephron* **2018**, *138*, 48.
[8] W. Safi, A. Marco, D. Moya, P. Prado, E. Garreta, N. Montserrat, *Front. Cell Dev. Biol.* **2022**, *10*, 948395.
[9] R. A. Wimmer, A. Leopoldi, M. Aichinger, N. Wick, B. Hantusch, M. Novatchkova, J. Taubenschmid, M. Hämmerle, C. Esk, J. A. Bagley, D. Lindenhofer, G. Chen, M. Boehm, C. A. Agu, F. Yang, B. Fu, J. Zuber, J. A. Knoblich, D. Kerjaschki, J. M. Penninger, *Nature* **2019**, *565*, 505.
[10] E. Garreta, R. D. Kamm, S. M. Chuva de Sousa Lopes, M. A. Lancaster, R. Weiss, X. Trepat, I. Hyun, N. Montserrat, *Nat. Mater.* **2021**, *20*, 145.
[11] M. Takasato, P. X. Er, H. S. Chiu, B. Maier, G. J. Baillie, C. Ferguson, R. G. Parton, E. J. Wolvetang, M. S. Roost, S. M. Chuva de Sousa Lopes, M. H. Little, *Nature* **2015**, *526*, 564.
[12] R. Morizane, A. Q. Lam, B. S. Freedman, S. Kishi, M. T. Valerius, J. V. Bonventre, *Nat. Biotechnol.* **2015**, *33*, 1193.
[13] E. Garreta, P. Prado, C. Tarantino, R. Oria, L. Fanlo, E. Martí, D. Zalvidea, X. Trepat, P. Roca-Cusachs, A. Gavaldà-Navarro, L. Cozzuto, J. M. Campistol, J. C. Izpisúa Belmonte, C. Hurtado Del Pozo, N. Montserrat, *Nat. Mater.* **2019**, *18*, 397.
[14] J. M. Rhodes, M. Simons, *J. Cell. Mol. Med.* **2007**, *11*, 176.
[15] S. Grebenyuk, A. Ranga, *Front. Bioeng. Biotechnol.* **2019**, *7*, 39.
[16] E. Garreta, R. Oria, C. Tarantino, M. Pla-Roca, P. Prado, F. Fernández-Avilés, J. M. Campistol, J. Samitier, N. Montserrat, *Mater. Today* **2017**, *20*, 166.
[17] E. Garreta, L. de Oñate, M. E. Fernández-Santos, R. Oria, C. Tarantino, A. M. Climent, A. Marco, M. Samitier, E. Martínez, M. Valls-Margarit, R. Matesanz, D. A. Taylor, F. Fernández-Avilés, J. C. Izpisua Belmonte, N. Montserrat, *Biomaterials* **2016**, *98*, 64.
[18] J. P. Guyette, J. M. Charest, R. W. Mills, B. J. Jank, P. T. Moser, S. E. Gilpin, J. R. Gershlak, T. Okamoto, G. Gonzalez, D. J. Milan, G. R. Gaudette, H. C. Ott, *Circ. Res.* **2016**, *118*, 56.
[19] S. E. Gilpin, X. Ren, T. Okamoto, J. P. Guyette, H. Mou, J. Rajagopal, D. J. Mathisen, J. P. Vacanti, H. C. Ott, *Ann. Thorac. Surg.* **2014**, *98*, 1721.
[20] X. Ren, P. T. Moser, S. E. Gilpin, T. Okamoto, T. Wu, L. F. Tapias, F. E. Mercier, L. Xiong, R. Ghawi, D. T. Scadden, D. J. Mathisen, H. C. Ott, *Nat. Biotechnol.* **2015**, *33*, 1097.
[21] K. H. Nakayama, C. C. Lee, C. A. Batchelder, A. F. Tarantal, *PLoS One* **2013**, *8*, e64134.
[22] C. A. Batchelder, M. L. Martinez, A. F. Tarantal, *PLoS One* **2015**, *10*, e0143849.
[23] M. Sambi, T. Chow, J. Whiteley, M. Li, S. Chua, V. Raileanu, I. M. Rogers, *Stem Cell Rev. Rep.* **2017**, *13*, 513.
[24] C. Du, K. Narayanan, M. F. Leong, M. S. Ibrahim, Y. P. Chua, V. M. Khoo, A. C. Wan, *Adv. Healthcare Mater.* **2016**, *5*, 2080.
[25] J. J. Song, H. C. Ott, *Trends Mol. Med.* **2011**, *17*, 424.
[26] R. J. Nagao, J. Xu, P. Luo, J. Xue, Y. Wang, S. Kotha, W. Zeng, X. Fu, J. Himmelfarb, Y. Zheng, *Tissue Eng., Part A* **2016**, *22*, 1140.

[27] M. Ali, A. K. Pr, J. J. Yoo, F. Zahran, A. Atala, S. J. Lee, *Adv. Healthcare Mater.* **2019**, *8*, e1800992.
[28] R. Sobreiro-Almeida, M. Gómez-Florit, R. Quinteira, R. L. Reis, M. E. Gomes, N. M. Neves, *Biofabrication.* **2021**, *13*, 45006.
[29] J. Su, S. C. Satchell, R. N. Shah, J. A. Wertheim, *J. Biomed. Mater. Res., Part A* **2018**, *106*, 2448.
[30] G. Remaggi, F. Barbaro, G. Di Conza, G. Trevisi, C. Bergonzi, R. Toni, L. Elviri, *Tissue Eng., Part C* **2022**, *28*, 148.
[31] N. J. Hogrebe, J. W. Reinhardt, K. J. Gooch, *J. Biomed. Mater. Res., Part A* **2017**, *105*, 640.
[32] X. Zhang, X. Chen, H. Hong, R. Hu, J. Liu, C. Liu, *Bioact. Mater.* **2021**, *10*, 15.
[33] J. W. Kim, S. A. Nam, J. Yi, J. Y. Kim, J. Y. Lee, S. Y. Park, T. Sen, Y. M. Choi, J. Y. Lee, H. L. Kim, H. W. Kim, J. Park, D. W. Cho, Y. K. Kim, *Adv. Sci.* **2022**, *9*, e2103526.
[34] Y. Kitamoto, H. Tokunaga, K. Tomita, *J. Clin. Invest.* **1997**, *99*, 2351.
[35] B. Phipson, P. X. Er, A. N. Combes, T. A. Forbes, S. E. Howden, L. Zappia, H. J. Yen, K. T. Lawlor, L. J. Hale, J. Sun, E. Wolvetang, M. Takasato, A. Oshlack, M. H. Little, *Nat. Methods* **2019**, *16*, 79.
[36] H. Wu, K. Uchimura, E. L. Donnelly, Y. Kirita, S. A. Morris, B. D. Humphreys, *Cell Stem Cell* **2018**, *23*, 869.
[37] J. H. Low, P. Li, E. G. Y. Chew, B. Zhou, K. Suzuki, T. Zhang, M. M. Lian, M. Liu, E. Aizawa, C. Rodriguez Esteban, K. S. M. Yong, Q. Chen, J. M. Campistol, M. Fang, C. C. Khor, J. N. Foo, J. C. Izpisua Belmonte, Y. Xia, *Cell Stem Cell* **2019**, *25*, 373.
[38] S. M. Czerniecki, N. M. Cruz, J. L. Harder, R. Menon, J. Annis, E. A. Otto, R. E. Gulieva, L. V. Islas, Y. K. Kim, L. M. Tran, T. J. Martins, J. W. Pippin, H. Fu, M. Kretzler, S. J. Shankland, J. Himmelfarb, R. T. Moon, N. Paragas, B. S. Freedman, *Cell Stem Cell* **2018**, *22*, 929.
[39] T. Mohamed, M. L. S. Sequeira-Lopez, *Semin. Cell Dev. Biol.* **2019**, *91*, 132.
[40] M. Anguiano, X. Morales, C. Castilla, A. R. Pena, C. Ederra, M. Martínez, M. Ariz, M. Esparza, H. Amaveda, M. Mora, N. Movilla, J. M. G. Aznar, I. Cortés-Domínguez, C. Ortiz-de-Solorzano, *PLoS One* **2020**, *15*, e0220019.
[41] M. G. McCoy, B. R. Seo, S. Choi, C. Fischbach, *Acta Biomater.* **2016**, *44*, 200.
[42] G. G. Giobbe, C. Crowley, C. Luni, S. Campinoti, M. Khedr, K. Kretzschmar, M. M. De Santis, E. Zambaiti, F. Michielin, L. Meran, Q. Hu, G. van Son, L. Urbani, A. Manfredi, M. Giomo, S. Eaton, D. Cacchiarelli, V. S. W. Li, H. Clevers, P. Bonfanti, N. Elvassore, P. De Coppi, *Nat. Commun.* **2019**, *10*, 5658.